journal homepage: www.brodogradnja.fsb.hr

Brodogradnja

An International Journal of Naval Architecture and Ocean Engineering for Research and Development

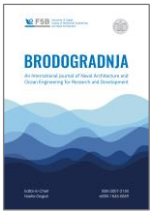

Short-term prediction of trimaran load based on data driven technology

Haoyun Tang[1], *Rui Zhu*[1], *Qian Wan*[2,3*], *Deyuan Ren*[1]

[1] *Navigation College, Dalian Maritime University, Dalian 116026, China*
[2] *College of Shipbuilding Engineering, Harbin Engineering University, Harbin 150001, China*
[3] *Dalian shipbuilding industry Co., Ltd, Dalian 116026, China*

ARTICLE INFO

Keywords:
Trimaran
Wave load
LSTM neural network
Signal decomposition

ABSTRACT

Due to the complex flow interference by side hulls, load prediction has been one of the obstacles to achieve structural health monitoring and intelligent navigation of trimarans. According to the machine learning theory, a short-term prediction method towards trimaran loads is studied by using an optimized data-driven model. In the research, the monitoring data from a trimaran model test is applied for the training and testing of long short-term memory (LSTM) neural network. The impact analysis on the factors such as input length, neuron number, artificial neural network (ANN) optimizer, and output scope, are taken. To highlight the trimaran high-frequency load fluctuation and improve the prediction accuracy, the LSTM neural network combines with different signal decomposition algorithms, such as Empirical Mode Decomposition (EMD), Ensemble Empirical Mode Decomposition (EEMD), Complete Ensemble Empirical Mode Decomposition with Adaptive Noise (CEEMDAN), and Variational Mode Decomposition (VMD). Through the comprehensive comparison of statistical indicators at different positions and wave environment, the VMD-LSTM model is selected by considering its highest load prediction ability among these artificial neural network models. The research will improve the load prediction accuracy in the structural health monitoring systems and offer effective technical support for intelligent unmanned trimarans.

1. Introduction

Trimaran has become an important maritime transportation tool, and its structural safety is crucial for the completion of the maritime missions, such as sea rescue, and tourism. However, some imperceptible damages in hull structures often occur during the long-term navigation of trimarans. To effectively monitor

* Corresponding author.
E-mail address: wanqian2022@126.com

http://dx.doi.org/10.21278/brod76101

Received 14 August 2024; Received in revised form 26 September 2024; Accepted 03 October 2024
Available online 16 October 2024
ISSN 0007-215X; eISSN 1845-5859

trimaran navigational status and warn on structural damages, the theoretical prediction based on potential flow theory and computational fluid dynamics (CFD) are often applied in trimarans. Jiang [1] investigated the trimaran motion and aerodynamic load by a series of CFD simulations. Then, Jiang [2] used a numerical lid to improve the trimaran motion prediction. Khoob [3] combined the finite element method with MAESTRO-Wave code to predict the trimaran motion and load. Tang [4] developed a nonlinear trimaran load prediction model by using the time-domain Rankine method. Zhang [5] combined CFD with the potential flow theory to assess trimaran roll motion in waves. Li [6] developed a PID control scheme in CFD to achieve trimaran self-navigation in oblique waves. Although the theoretical prediction can predict ship motion and load in ideal wave cases, a gap still exists considering the uncertainty and irregularity of waves in actual ocean environment, especially for high-frequency loads. Additionally, the wave impact on hull structures cannot be reflected rapidly when the real-time changes in external wave condition happen. The complicated signal fluctuation poses significant challenges for the real-time evaluation on hull structural state. It is also one of the critical technical difficulties for the achievement of trimaran's structural health in autonomous operation.

With the widespread application of artificial intelligence technology in ship engineering, the concept of intelligent unmanned trimaran is proposed and implemented by using structural health monitoring systems. In the monitoring systems, the signals of ship motion and load are collected to establish a data-driven model and predict the fluctuation of load and structural state in short-term future [7]. The data-driven signal prediction technology has been developed rapidly by scholars in ship engineering [8]. Due to the limitation of high-frequency sensors, scholars mainly focused on predicting ship motion in an early stage. Kaplan [9] combined the monitored wave data at ship bow and convolution algorithms to establish a data-driven model and realize the prediction of ship motion. Zeng [10] developed a data-driven model based on radial basis function network and predicted ship motion attitude by the historical motion data. Sun [11] also investigated the prediction of ship motion attitude by a data-driven model based on LSTM neural network and gaussian process regression. Presti [12] used a physics-oriented neural network in modelling the ship maneuvering process. Then, Jiang [13] developed a data-driven forecast method for KCS ship motion by using LSTM neural network and Golden jackal optimization. Gao [14] combined the improved empirical mode decomposition with a dynamic residual recurrent neural network based on the bidirectional structure and time pattern attention mechanism to realize the prediction of real-time ship motion. With the increasing demand for structure health monitoring (SHM) in ship engineering, the data-driven signal prediction technology gradually spread from monohull's motion to multihull's load and structure response [15]. Wu [16] combined complementary ensemble empirical mode decomposition (CEEMD) and support vector machine (SVM) to established a data-driven model to forecast the stress fluctuation in ship structures successfully. Chao [17] developed a LSTM data-driven model to predict hull sectional loads in various wave cases. Tang [18] optimized the LSTM data-driven model by using Bayesian algorithm to preliminary achieve the trimaran load prediction. To predict different types of ship loads in real-time, Wang [19] applied recurrent neural network (RNN) and error correction strategy in the establishment of the data-driven load model. Then, Wang [20] also took a comparative analysis of different recurrent neural networks for load prediction under the varied noise impact. Through a series of research, the data-driven load prediction has been preliminarily proven to be feasible by using artificial neural networks (ANNs). But the optimization of data-driven load prediction model is still one of the challenges in improving high-frequency load prediction accuracy at present. For trimarans, due to the flow interference of side hulls, the monitoring load signal of trimarans are always more complicated than that of monohulls, which contains more high-frequency components along the ship length and further increases the load forecasting difficulty with high precision. Therefore, it is necessary to develop an optimized data-driven model for trimaran load.

In the research, a trimaran load prediction method based on the data driven technology is investigated. The LSTM neural network is used as the core to construct the data-driven load prediction model, and it is trained by the load data from a trimaran scaled model test. To optimize this data-driven load prediction model, the influence on the parameters such as input length, neuron number, ANN optimizer, and output scope, is analyzed. Then, the data-driven model is further improved by combing the optimized LSTM neural network with some signal decomposition algorithms, such as empirical mode decomposition, ensemble empirical mode decomposition, complete ensemble empirical mode decomposition with adaptive noise, and variational mode decomposition. Finally, the VMD-LSTM load prediction model is selected through the comparative analysis.

This research is the foundation for monitoring signal diagnosis and fault identification in intelligent trimaran monitoring systems, and it also offer some reliable technical support for autonomous navigation of high-speed unmanned trimarans.

2. Monitoring signal decomposition

When trimaran is sailing in irregular waves, the monitoring signal shows an intricate hybrid fluctuation [21]. This fluctuation always includes a large number of high-frequency components, which are mainly caused by random noise, instantaneous bow slamming and green water. The hybrid fluctuation phenomenon in raw monitoring signal will enhance the difficulty of ANNs in understanding the rule of signal fluctuations and finally lead to the misjudgment of monitoring signal trend in the data-driven prediction load model. Therefore, some signal decomposition algorithms are often applied to extract valuable features from the raw monitoring signal [22]. The combination framework of signal decomposition and ANNs is shown in Fig. 1. In the ship engineering, the common signal decomposition methods mainly include empirical mode decomposition, ensemble empirical mode decomposition, complete ensemble empirical mode decomposition with adaptive noise, and variational mode decomposition. Due to the differences in decomposition frameworks, these signal decomposition methods both have an undeniable impact on the extraction of signal characteristics.

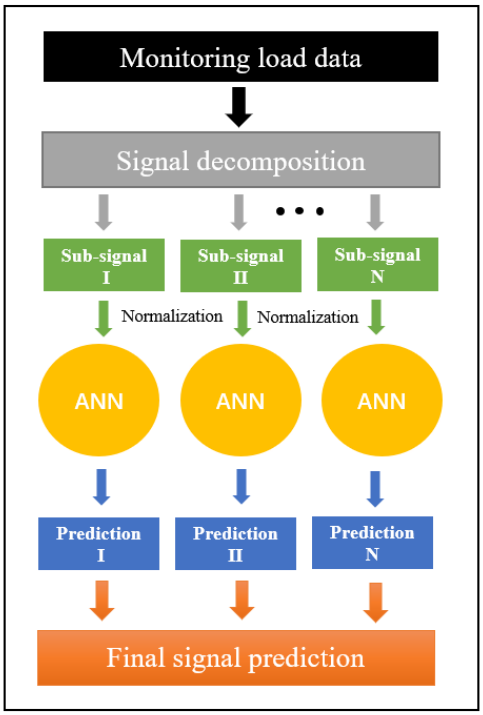

Fig. 1 Combination framework of signal decomposition and ANNs

2.1 Empirical mode decomposition

Empirical mode decomposition is a traditional time-domain signal processing algorithm that has advantages in handling nonstationary and nonlinear signal [23]. In the EMD, the raw signal $H(t)$ can be represented by a series of intrinsic mode functions (IMFs) χ_i and residual error S_n:

$$H(t) = \sum_{i=1}^{n} \chi_i(t) + S_n(t) \tag{1}$$

where i denotes the layer of mode decomposition; n is the total layer number of mode decomposition; t is the monitoring time. To calculate the IMFs, the local extremum of monitoring signal is searched. The upper and lower envelopes are calculated through interpolation and fitting. Then, the mean envelope E_M is obtained:

$$E_M(t) = [E_U(t) + E_D(t)]/2 \tag{2}$$

where E_U and E_D denote upper and lower envelopes, respectively. The potential intrinsic mode function I is calculated:

$$I(t) = H(t) - E_M(t) \tag{3}$$

The IMFs must follow some basic conditions: (i) the number of local extremum and the number of zero-crossing in the entire time range must either equal or differ at most by one.; (ii) the mean value of the upper and the lower envelope must be zero. If the potential function meets these conditions, the value of potential function is the same with the IMFs. If the potential function cannot meet the above requirements, the signal $H(t)$ is further updated by the potential function. Eq. 3 is applied repeatedly until the IMFs are found. The residue $R(t)$ is also obtained:

$$R(t) = H(t) - \chi(t) \tag{4}$$

Then, the residue $R(t)$ is considered as a new signal to take the mode decomposition process of Eq. 2~3 again. In this cyclic calculation, the IMFs at different signal mode layers are found. The signal decomposition process will finally stop, when the residue becomes a monotonic function or a constant. In essence, the EMD method analyzes the monitoring signal by decomposing the fluctuation into different IMFs. Herein, the calculated IMFs are a series of sub-signal sequences with different characteristic scales.

2.2 Ensemble empirical mode decomposition

Although the EMD has some advantages in handling instable signal sequences, there are some drawbacks caused by the uneven distribution of extreme points. The mode mixing phenomenon often occurs in the EMD [24]. To prevent these drawbacks, ensemble empirical mode decomposition is proposed by combining the EMD with a noise-assisted data analysis. In the EEMD, a series of Gaussian noises $\bar{n}_k$ (k=1~M) is added to the raw signal $H(t)$ to alter the initial signal characteristics:

$$\bar{H}_k(t) = H(t) + \bar{n}_k(t) \tag{5}$$

Then, the EMD cyclic calculation is also taken for the new signal $\bar{H}_k$ to obtain corresponding IMFs. Due to the different noise addition, there are multiple IMFs at each time scale. The mean value of these IMFs $\bar{\chi}_i^j(t)$ is calculated as the final IMF:

$$\bar{\chi}_i(t) = \frac{1}{M}\sum_{k=1}^{M} \bar{\chi}_i^k(t) \tag{6}$$

In the EEMD, the Gaussian distribution spectrum in the additional noise is utilized to automatically distribute the signals of different time scales to the appropriate reference scales.

2.3 Complete ensemble empirical mode decomposition with adaptive noise

The EEMD improves the mode mixing phenomenon in EMD, but the noise added in the raw signal cannot be eliminated completely. Its reconstruction signal error has a significant dependence on the number of noise addition. To reduce reconstruction errors, a complete ensemble empirical mode decomposition with adaptive noise is developed. In the CEEMDAN, the Gaussian noise $\hat{n}_k$ is also added into the raw signal $H(t)$, but an extra noise coefficient ε_0 is introduced to control the noise addition:

$$\hat{H}_j(t) = H(t) + \varepsilon_0 \hat{n}_k(t) \tag{7}$$

The IMF and residue at first mode are still obtained by averaging all the components:

$$\hat{\chi}_1 = \frac{1}{M}\sum_{k=1}^{M}\hat{\chi}_1^k \tag{8}$$

$$\hat{R}_1(t) = \hat{H}(t) - \hat{\chi}_1(t) \tag{9}$$

Then, IMF and residue at second mode can be calculated as follow:

$$\hat{\chi}_2 = \frac{1}{M}\sum_{k=1}^{M} EMD_1[\hat{R}_1(t) + \varepsilon_1 EMD_1(\hat{n}_k)] \tag{10}$$

$$\hat{R}_2(t) = \hat{H}(t) - \hat{\chi}_2(t) \tag{11}$$

Similarly, the residue and IMF at following modes can be further obtained:

$$\hat{R}_m(t) = \hat{H}(t) - \hat{\chi}_m(t) \tag{12}$$

$$\hat{\chi}_{m+1} = \frac{1}{M}\sum_{k=1}^{M} EMD_1[\hat{R}_m(t) + \varepsilon_m EMD_m(\hat{n}_k)] \tag{13}$$

where $\hat{R}_m$ denotes the m-th residue, and $\hat{\chi}_{m+1}$ is the IMF at (m+1)-th model. $EMD_m(\cdot)$ is the function to extract the m-th IMFs based on the EMD algorithm. The calculation will be repeated by Eq. 12~Eq. 13 until the residue meet the criterion:

$$\sum_{j=1}^{M}\frac{\left|\hat{R}_{m-1} - \hat{R}_m\right|}{\hat{R}_{m-1}^2} \le \gamma \tag{14}$$

Herein, the calculation termination coefficient γ is set to 0.2 for general engineering application.

2.4 Variational mode decomposition

Variational mode decomposition is a non-recursive algorithm proposed by Dragomiretskiy [25] to analyze signal characteristics. Its theoretical framework can control the number of decomposed mode functions while effectively suppress the mode mixing phenomenon. In the VMD, the raw signal $H(t)$ is divided into a series of band-limited intrinsic mode functions u_i (i=1~K). These IMFs has a center pulsation ω_i, and its bandwidth is estimated in Gaussian smoothness. Then, the constrained variational condition is taken:

$$\begin{aligned} &\min_{\{u_i\},\{\omega_i\}}\left\{\left\|\partial_t\{[\delta(t)+\frac{j}{\pi t}]*u_i(t)\}e^{-j\omega_i t}\right\|_2^2\right\} \\ &\text{subject to}\quad \sum_{i=1}^{K}u_i(t) = H(t) \end{aligned} \tag{15}$$

where $\delta(t)$ is the unit impulse function, j is the imaginary unit, and $*$ denotes the convolution. To solve the constrained condition, the quadratic penalty and Lagrange multipliers are applied:

$$L(\{u_i\},\{\omega_i\},\lambda)=\alpha\sum_{i=1}^{K}\left\|\partial_t\{[\delta(t)+\frac{j}{\pi t}]*u_i(t)\}e^{-j\omega_i t}\right\|_2^2 + \left\|H(t)-\sum_{i=1}^{K}u_i(t)\right\|_2^2+\left\langle\lambda(t),H(t)-\sum_{i=1}^{K}u_i(t)\right\rangle \tag{16}$$

where α is the bandwidth parameter, and $\lambda(t)$ denotes the Lagrange multiplier. For the quadratic optimization of these related parameters in the VMD, the frequency domain solution is updated by using Fourier transform and wiener filtering:

$$\tilde{u}_i^{l+1}(\omega)=\frac{\tilde{H}(\omega)-\sum_{m=1,m<i}^{K}\tilde{u}_m^{l+1}(\omega)-\sum_{m=1,m>i}^{K}\tilde{u}_m^{l}(\omega)+\left[\tilde{\lambda}^l(\omega)/2\right]}{1+2\alpha(\omega-\omega_i^l)^2} \tag{17}$$

$$\omega_i^{l+1}=\frac{\int_0^\infty \omega|\tilde{u}_i^{l+1}(\omega)|^2\,d\omega}{\int_0^\infty|\tilde{u}_i^{l+1}(\omega)|^2\,d\omega} \tag{18}$$

$$\tilde{\lambda}^{l+1}(\omega)=\tilde{\lambda}^l(\omega)+\gamma[\tilde{H}(\omega)-\sum_{i=1}^{K}\tilde{u}_i^{l+1}(\omega)] \tag{19}$$

where l is the iteration number, γ is the fidelity coefficient, $\tilde{u}(\omega)$, $\tilde{\lambda}(\omega)$, $\tilde{H}(\omega)$ denote the Fourier transform of $u(t)$, $\lambda(t)$, and $H(t)$, respectively. Finally, The IMFs are obtained by using the inverse Fourier transform.

3. Artificial neural network

Artificial Neural Networks are the computational models that imitate the structure and functioning principles of human brains. They consist of numerous interconnected neurons and form an operational network. ANNs will generate outputs by summing the weights and applying the activation functions, after the network receives input information and transmits it to each neuron for learning [26]. Currently, there are various types of ANNs, such as back propagation (BP) neural network, convolutional neural network (CNN), and LSTM neural network. Among them, LSTM neural network has advantages in the time-domain signal sequence prediction, Therefore, this research used the LSTM neural network as the core algorithm to establish a data-driven model for short-term load forecasting of trimarans.

3.1 Long short-term memory neural networks

Long short-term memory neural network was proposed by Hochreiter and Schmidhuber [27]. This neural network, as an optimized intelligent algorithm of Recurrent Neural Network (RNN), effectively solve the issues of vanishing and exploding gradients. In the LSTM neural network, gates play a crucial role in controlling the information transmission and updating memory cells. These specific gates include input gate, forget gate, and output gate. Fig. 2 shows the structure of memory cells and gates in the LSTM hidden layer.

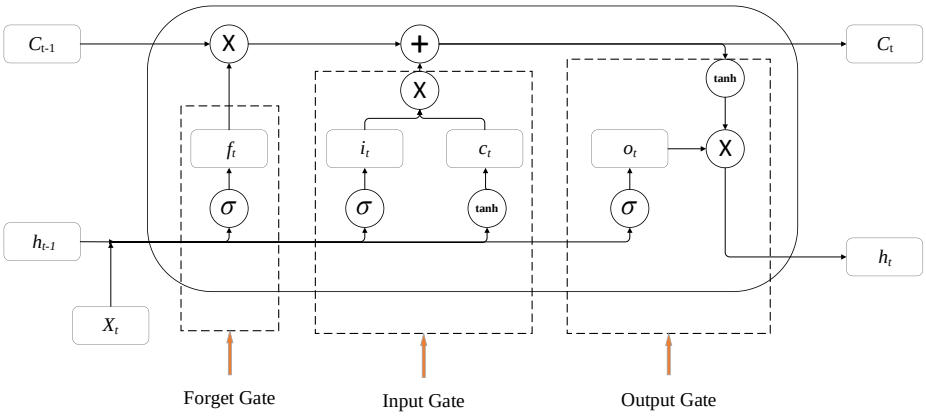

Fig.2 Structure of memory cells and gates in LSTM

For the forget gate of LSTM neural network, its function is to delete some outdated information from the memory cell. Then, the output vector f_t is calculated:

$$f_t = \sigma(W_f h_{t-1} + V_f X_t + b_f) \tag{20}$$

where X_t is the input of the LSTM neural network; h_{t-1} is the output of the previous time step; σ is the sigmoid activation function; W_f and V_f are the matrix weights for the output and input in forget gate; b_f is the bias matrix for the forget gate. The input gate is to determine whether to put new information into the memory cell, and its updated formula is also shown as follows.

$$i_t = \sigma(W_i h_{t-1} + V_i X_t + b_i) \tag{21}$$

$$s_t = \tanh(W_s h_{t-1} + V_s X_t + b_s) \tag{22}$$

$$C_t = f_t \odot C_{t-1} + i_t \odot s_t \tag{23}$$

where W_i and V_i are the matrix weights of the output and input for the LSTM input gate; tanh represents the hyperbolic tangent function; W_s and V_s denote the candidate memory matrix weights of the output and input in the input gate. b_i and b_s are the bias matrix and candidate memory bias matrix for the input gate; $\odot$ denotes the Hadamard product. According to the updated information in the memory cell, the output gate can adjust the output component:

$$o_t = \sigma(W_o h_{t-1} + V_o X_t + b_o) \tag{24}$$

where W_o and V_o are the matrix weights of output and input for the output gate, respectively. b_o denotes the bias matrix for the output gate. The final output of LSTM neural network at the current time step is obtained:

$$h_t = \tanh(C_t) \odot o_t \tag{25}$$

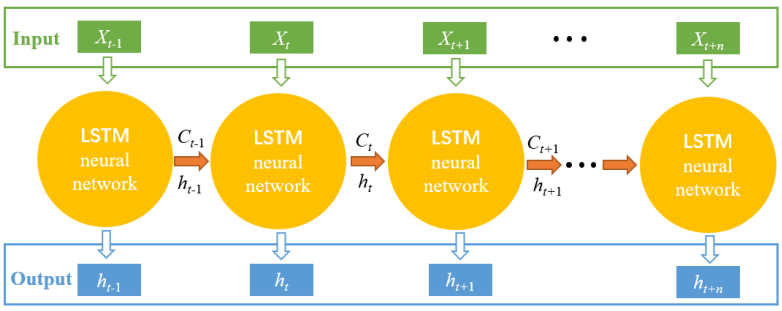

Fig. 3 Sketch of signal sequence prediction based on LSTM neural network.

According to the gate mechanism, the LSTM neural network can effectively control the information in the memory cell and autonomously adjust its prediction ability in signal sequences. The specific LSTM prediction sketch in signal sequences is shown in Fig. 3.

3.2 Optimization of artificial neural networks

The training of LSTM neural network plays a crucial role in LSTM prediction performance. In the training, the relevant parameters of LSTM neural network will be continuously updated to find the optimal solution for eliminating the error between expectation and prediction. To further accelerate convergence and improve the efficiency of LSTM training, the ANN optimizers based on the gradient descent optimization algorithms are combined with the LSTM neural network in the research.

3.2.1 Stochastic Gradient Descent with Momentum

Stochastic Gradient Descent with Momentum (SGDM) is an improved version of the Stochastic Gradient Descent (SGD) algorithm that incorporates the concept of momentum optimization. The main purpose of the added momentum optimization is to accelerate convergence and reduce oscillations during gradient descent, especially in flat regions and valleys of the parameter space. The SGDM introduces a momentum term v to consider the previous gradient direction when the LSTM parameter updates. The momentum term, as a weighted moving average of gradients, is controlled by the momentum parameter β. In the SGDM, the gradients of the current sample are calculated, and the parameter θ are updated by incorporating the previous momentum term:

$$v_r = \beta v_{r-1} + (1-\beta)\nabla J(\theta_r) \tag{26}$$

$$\theta_{r+1} = \theta_r - \eta v_r \tag{27}$$

where r denotes the iteration number; J is the gradient function of the current mini-batch sample; η is the global learning rate of LSTM. The SGDM algorithm allows acceleration of the parameter updating when the gradient direction remains consistent. It also reduces oscillations when the gradient direction changes. Finally, the application of SGDM will improve the stability of gradient convergence.

3.2.2 Root Mean Square Propagation

Root Mean Square Propagation (RMSProp) is an adaptive optimized method to select learning rates in the stochastic gradient descent. The RMSProp can adjust the learning rates based on the historical gradient information and also consider the iterative decay. The vector parameter $\bar{v}$ and target parameter $\bar{\theta}$ in the RMS Prop are updated as follows.

$$\bar{v}_{r+1} = \begin{cases} \bar{\alpha}\bar{v}_r + (1-\bar{\alpha})g_r^2 & r > 0 \\ g_0^2 & r = 0 \end{cases} \tag{28}$$

$$\bar{\theta}_{r+1} = \bar{\theta}_r - \frac{\eta}{\sqrt{\bar{\theta}_{r+1} + \varepsilon}} g_r \tag{29}$$

where $\bar{\alpha}$ is the attenuation coefficient and set to 0.9 in the research; ε is the small constant to prevent division by zero in Eq. 29. g_r^2 denotes the Hadamard calculation of $g_r \odot g_r$, and the gradient parameter g_r is also calculated by the gradient function:

$$g_r = \nabla J(\bar{\theta}_r) \tag{30}$$

The RMSProp algorithm can reduce the gradient oscillation of the computational path to the minimum, while allowing for a higher learning rate to accelerate the learning speed in LSTM.

3.2.3 Adaptive Moment Estimation

Adaptive Moment Estimation (Adam) method is developed by combining the advantages of SGDM and RMSProp [28]. This algorithm can solve some typical problems in gradient descent, such as random small sample, adaptive learning rate, and local small gradient traps. In the *r*-th iteration, the exponential moving average value $\hat{m}$ and squared gradient $\hat{v}$ are estimated by the first and second moment:

$$\hat{m}_r = \hat{\beta}_1 \hat{m}_{r-1} + (1-\hat{\beta}_1) g_r \tag{31}$$

$$\hat{v}_r = \hat{\beta}_2 \hat{v}_{r-1} + (1-\hat{\beta}_2) g_r^2 \tag{32}$$

Herein, the momentum parameters $\hat{\beta}_1$ and $\hat{\beta}_2$ decide the decay rate of these moving average values. In general applications, the parameters $\hat{\beta}_1$ and $\hat{\beta}_2$ are set to 0.9 and 0.999. The initial bias correction term is also applied, then the bias-corrected first and second moments ($\hat{m}_r^*$ and $\hat{v}_r^*$) are further updated:

$$\hat{m}_r^* = \hat{m}_r / (1-\hat{\beta}_1^r) \tag{33}$$

$$\hat{v}_r^* = v_r / (1-\hat{\beta}_2^r) \tag{34}$$

Finally, the target parameter $\hat{\theta}$ are obtained as follows.

$$\hat{\theta}_{r+1} = \hat{\theta}_r - \frac{\eta}{\sqrt{\hat{v}_{r+1}^* + \varepsilon}} \hat{m}_r^* \tag{35}$$

The Adam algorithm has high computational efficiency and low memory requirement in comparison with the common gradient optimization methods. The combination of Adam and LSTM has a wide application scenario.

4. Establishment and analysis of trimaran load prediction model

In order to establish a data driven load prediction model, the monitoring load data from a series of trimaran model tests are extracted in Tang's research [29,30]. The scaled trimaran shell is divided into segments along ship length, and the hull stiffness distribution is simulated by using variable cross-section beams inside the model, as shown in Fig. 4.

The dual parameter spectrum recommended by the international ship structure conference (ISSC) was simulated in the towing tank. Table 1 shows the parameters of irregular wave conditions in the trimaran model test. Herein, H_S denotes the statistical characteristics value of wave height; T_Z is the zero-crossing period. The ship sailing speed in the wave condition WI is 20kn. Considering the limitation of the tank length in the model test, a single model sailing case in irregular waves cannot fully suffer the whole wave spectrum. Therefore, a series of irregular wave cases were taken to form the designed wave spectrum. For the wave condition WI, the total number of the sub-cases is 50. According to the scaling ratio (1:25) conversion, the actual ship suffered over 300 irregular sub-waves and lasts for 2 hours. Similarly, each irregular wave environment in the wave condition WII and WIII also adopts the combination of multiple sub-cases. The relative errors of wave height and zero-crossing period are both lower than 6%. The randomness requirement of irregular waves is also satisfied in the model test. When the trimaran model is sailing in irregular waves, the hydrodynamic pressure will motivate different movement in the model segments and cause vertical bending moment (VBM) of hull beam deformation. The fluctuations of VBM at different hull positions are monitored and recorded by the sensors installed on the hull beams [31]. The monitored VBM at bow, midship, and stern, are used as the trimaran load at the typical positions for the training and testing of LSTM neural network.

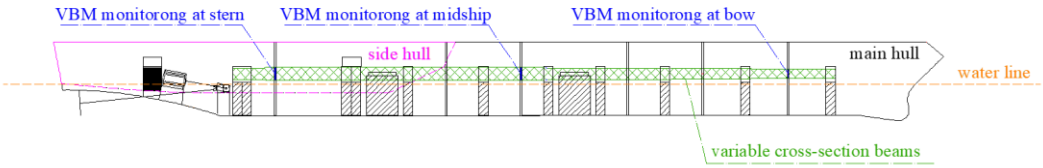

(a) trimaran load monitoring locations

(b) trimaran segmented model design

Fig. 4 Trimaran segmented model design

Table 1 Parameters of irregular wave conditions

Wave condition	H_S, m	T_Z, s	Ship speed, kn
WI	4.0	9.7	20
WII	4.2, 4.0, 3.8, 3.6	6.7	0
WIII	3.2	9.0	5,10,15

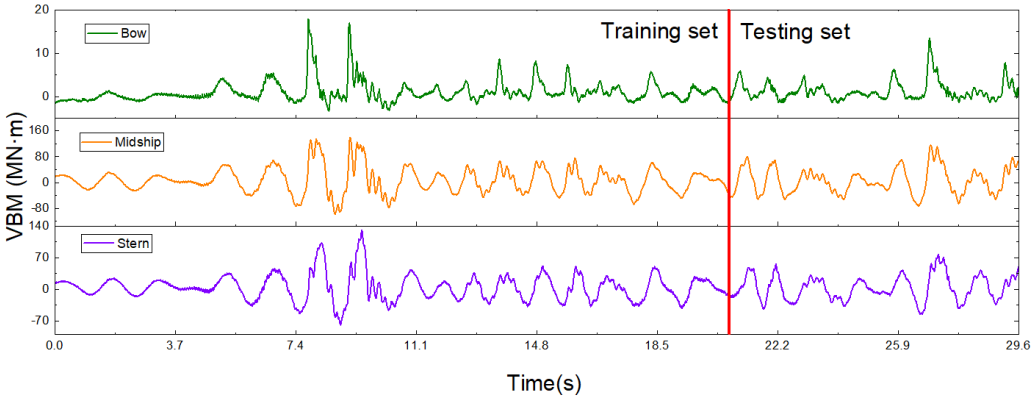

Fig. 5 Time histories of trimaran load at different monitoring positions (case WI)

Fig. 5 shows the monitored load fluctuation in a sub-cases of wave condition WI. Herein, the time are still in the model scale. Although the VBMs at the three monitoring positions have similar signal fluctuations, there are differences in high-frequency oscillations, peak steepness, and wave phase. In order to avoid the sharp decrease in prediction accuracy caused by the wave randomness, it is necessary to implement the strategies of online learning and regular updating in the data-driven prediction model during the actual ship navigation. Therefore, the sub-cases are defined as the intervals for the data-driven model updates, considering their potential differences. In these cases, the load data are divided into two parts: training set and testing set. The proportion of the training set and the testing set to the entire load dataset are 70% and 30%, respectively. The training set is used to build a LSTM data-driven model, and the accuracy and stability of the data-driven model were verified in the testing set. In the LSTM neural network, the max number of iterations is 200; the initial learning rate is defined as 0.001; the ridge regression regularization coefficient is 0.0003. These parameters of LSTM neural network are determined, according to the previous relevant research on LSTM neural networks [32, 33]. In the establishment of load prediction model, the designed sampling frequency is 50Hz and the time step is 0.02s. This sampling frequency can monitor the high-frequency load fluctuations

caused by springing and whipping. A prediction step size of 5~20 ahead is taken in load sequence. For the actual trimaran, the predicted load times in advance are 0.5 s~2.0 s, according to the scaling ratio (1:25) conversion. Although the forecast time is relatively short, it can basically cover the impact of a slamming and some wavelets. Under the 5-step ahead prediction, the influence of input length, neuron number, ANN optimizer, and output scope, are investigated. The LSTM neural network also combines with EMD, EEMD, CEEMDAN, and VMD, to improve load prediction accuracy. To assess the capability of these data-driven models, the relative root mean squared error (RRMSE) and the R-squared correlation coefficient are calculated as statistical indexes.

4.1 Impact analysis of input length

The input length of artificial neural networks always affects its prediction ability. The short length of input data makes it difficult for ANNs to recognize the characteristics and development trends of the monitoring signals, while the long input length will enormously increase the computational space and time consumption of ANNs. Therefore, the selection of input length is critical for the data-driven load prediction model. In the research, the input length W is set to 5, 10, 20, 50, and 100, respectively. The trimaran load prediction results with different input lengths are shown in Fig. 6.

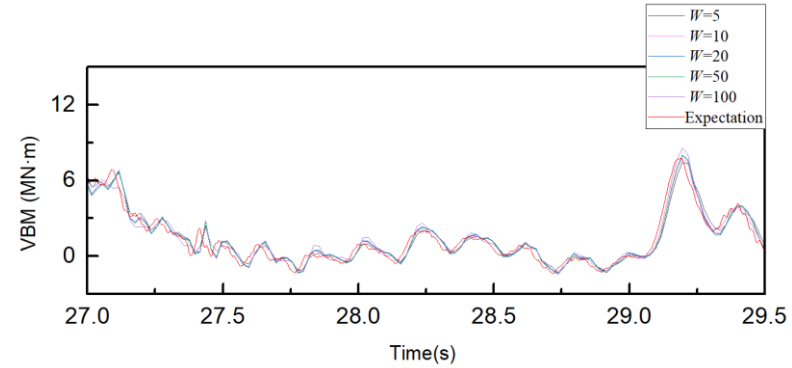

(a) Bow load prediction with different input lengths

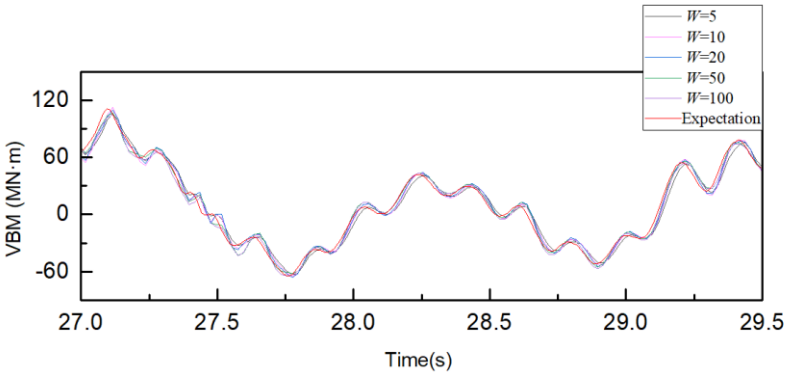

(b) Midship load prediction with different input lengths

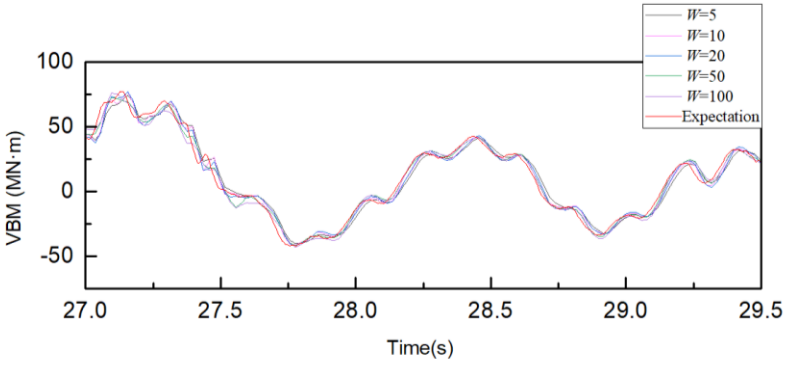

(c) Stern load prediction with different input lengths

Fig. 6 Trimaran load prediction results with different input lengths

Obviously, the data-driven model based on the LSTM neural network can roughly predict the trimaran load variations at bow, midship, and stern. The amplitude deviation between prediction and expectation is easier to find at load peaks. The phase deviations at bow and stern are relatively pronounced among these three monitoring positions. Fig. 7 shows the final statistical indicators under the varied input lengths. With the input length growth, the RRMSE and R-squared correlation coefficient both fluctuate, to some extent. At midship and stern, the min RRMSE and max R-Square coefficient are found when the input length is 50. But the input length for the min RRMSE and max R-Square coefficient is 100 at bow. The impact of input data length on trimaran load prediction is not same at the different monitoring positions. Because the complicated signal fluctuations caused by slamming and green water are included in the bow signal, the LSTM neural network needs more input volume to learn the characteristics of the bow load fluctuation. Although the amplitude of load fluctuation at midship and stern is larger than that at bow, the RRMSE results of midship and stern are relatively lower than the RRMSE results at bow. It is also shown that the R-squared correlation coefficients of midship are always higher than those of bow and stern in different input data lengths. Obviously, there is a stronger comprehension ability of the LSTM neural network towards the actual monitoring signal at midship. Considering the consistency of the input data duration obtained from actual monitoring systems, the input length is set to 50 in the subsequent LSTM optimization.

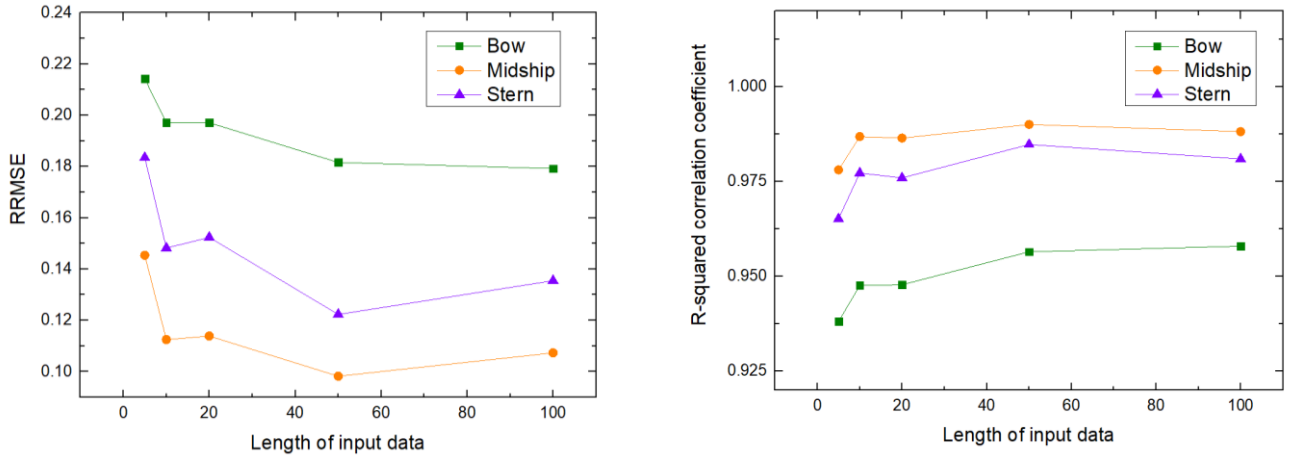

(a) Results of RRMSE (b) Results of R-squared correlation coefficient

Fig. 7 Statistical indicators under the varied input data lengths

4.2 Impact analysis of neuron quantity

For LSTM neural network, the number of neurons in hidden layer is also one of the critical parameters to determine its forecasting capability. In general, the increasing in the number of neurons can improve the learning and expression capabilities of LSTM neural network. However, the excessive neurons will also lead to the overfitting phenomenon and reduce the generalization ability of the prediction model.

To investigate the influence of different neuron quantities on the LSTM data-driven model, the number of neurons N is set to five values: 16, 32, 64, 128, and 256. The prediction results with different number of neurons are calculated and shown in Fig. 8. It is found that the sensitivity of the neural network's quantity to the forecast results is relatively low, although the changes in the hidden layer neurons can still cause variations in the load prediction results, especially for the high-frequency load peaks at bow.

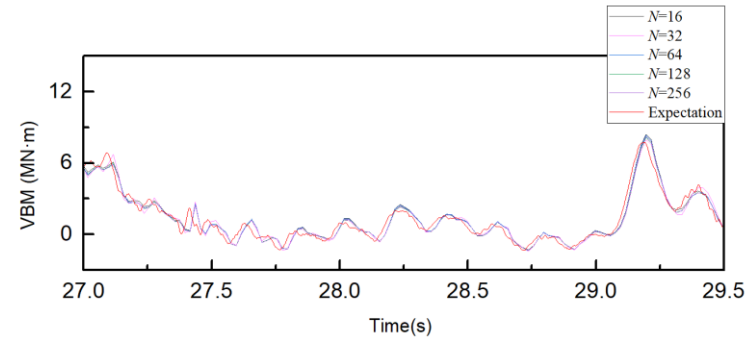

(a) Bow load prediction with different number of neurons

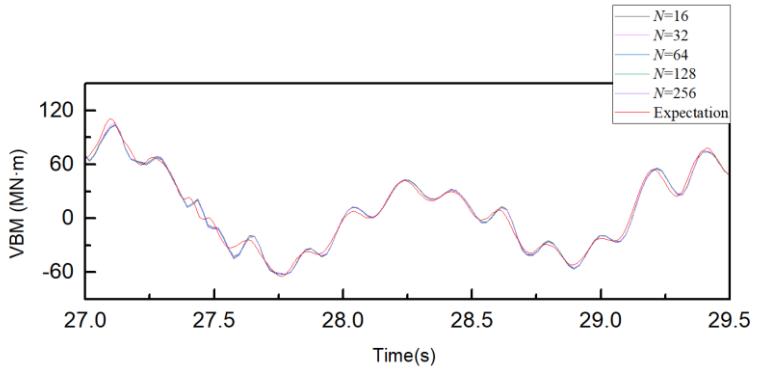

(b) Midship load prediction with different number of neurons

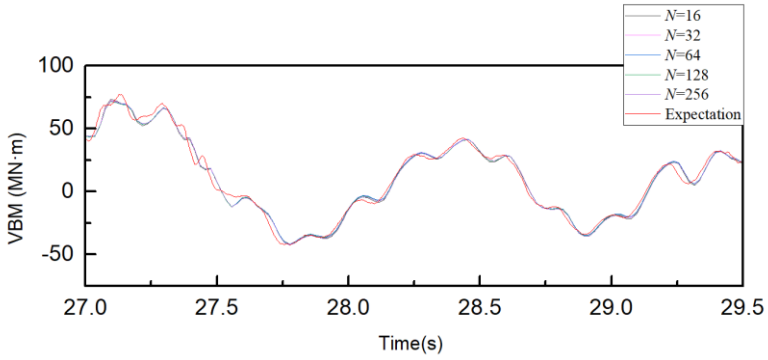

(c) Stern load prediction with different number of neurons

Fig. 8 Trimaran load prediction results with different number of neurons

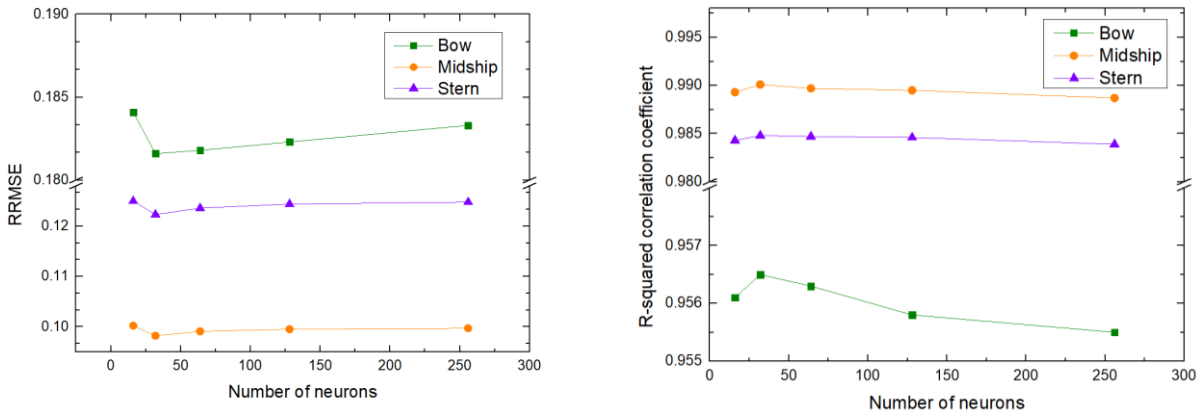

(a) Results of RMSE (b) Results of R-squared correlation coefficient

Fig. 9 Statistical indicators under varied number of neurons

Fig. 9 summarizes the statistical results of RRMSE and R-squared correlation coefficients with different number of neurons. With the number of neurons increasing, the RRMSE of the LSTM neural network at midship and stern declines initially and then converges gradually at the high neuron quantity. This rough convergence phenomenon is also found in the calculation of the R-squared correlation coefficients at midship and stern. But for the bow load perdition, the error rebound appears with the growth of neuron number. Due to the more pronounced high-frequency fluctuations in the bow load, the overfitting effect caused by the high neuron number may lead to the decrease in high-frequency load forecast accuracy. In comparison with the impact on the input length, the influence of neuron quantity is relatively small for trimaran load prediction. In addition, the neuron number growth will enhance the training time of the data driven model. When the neuron number increases from 32 to 256, the LSTM training times at bow, midship, and stern are delayed by 73.17%, 72.04%, and 82.38%, respectively. To save computing time and enhance prediction efficiency in the monitoring system, the number of neurons is set to 32 for general requirement of trimaran structural health assessment.

4.3 Impact analysis of ANN optimizer

To improve the accuracy and stability of LSTM neural networks, some optimization algorithms are always applied, such as Adam, RMSprop, and SGDM. In the framework of the LSTM neural network, the number of neurons and the input length is 32 and 50. The influence of different ANN optimizers are further studied by observing the predicted load fluctuations.

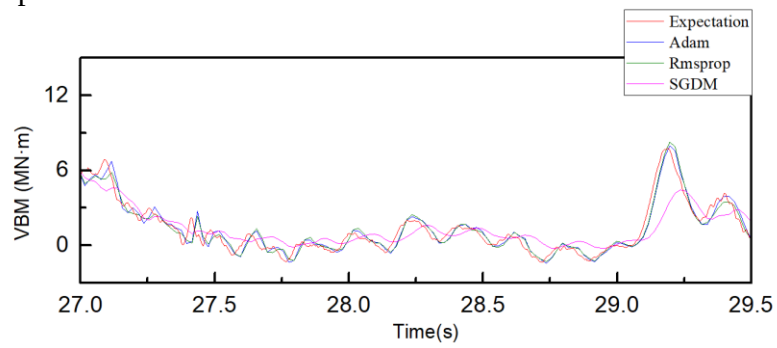

(a) Bow load prediction with different ANN optimizers

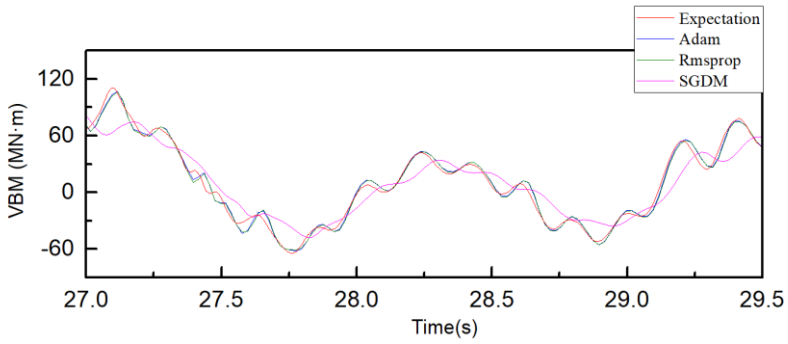

(b) Midship load prediction results with different ANN optimizers

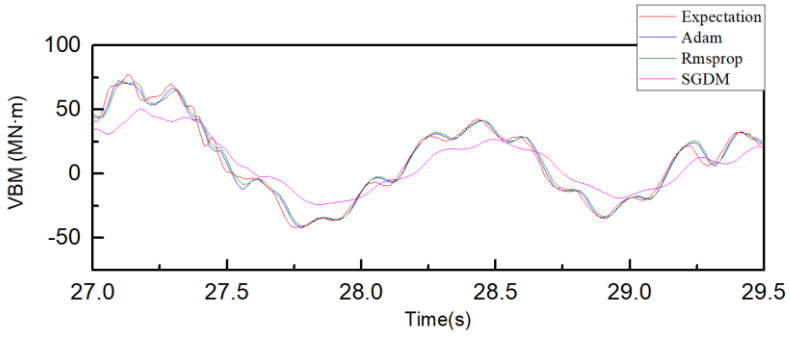

(c) Stern load prediction results with different ANN optimizers

Fig. 10 Trimaran load prediction results under different ANN optimization algorithms.

Fig. 10 shows the predicted load fluctuation under different ANN optimization algorithms. It is found that the SGDM optimization in LSTM neural network cannot improve the predicted precision and lead to some extra phase deviation in the trimaran load prediction. The Adam and the RMSprop optimizers have some similar advantages in improving the prediction of load amplitude.

Fig. 11 summarizes the statistical results of RRMSE and R-squared correlation coefficients with different ANN optimizers. Obviously, the SGDM optimizer gets the maximum of RRMSE and minimum of R-squared correlation coefficient among these ANN optimizers. The RRSME at bow is always higher than that of midship and stern, regardless of the varied optimizer application. In addition, the RRMSE results by the Adam optimizer are lower than that of the RMSprop optimizer, and the calculated R-squared correlation coefficient under the Adam optimizer increases by 1.56% in comparison with the R-squared coefficient of the RMSprop optimizer. Through comparative analysis, the Adam optimizer is more suitable for trimaran load prediction along the ship length.

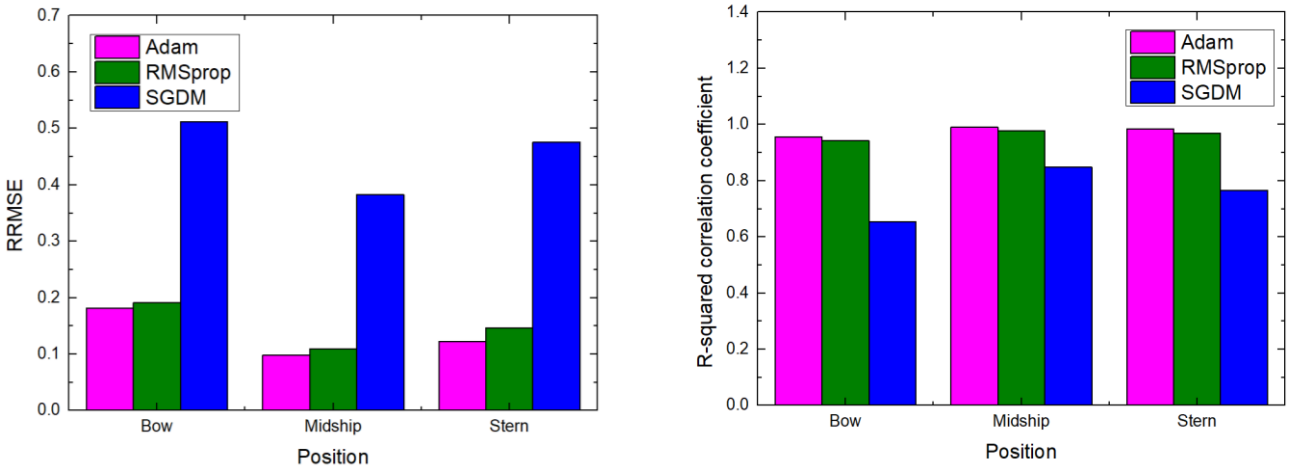

(a) Results of RRMSE (b) Results of R-squared correlation coefficient

Fig. 11 Statistical indicators at different ANN optimizers

4.4 Establishment and analysis of combined model

Although some optimizations on LSTM neural network have been carried, there are still some deviations between expectation and prediction in detail, especially at the trimaran bow and stern. Due to the bow slamming and the stern interference of side hulls, the trimaran load signal contains more high-frequency components at bow and stern, and these high-frequency vibration is also crucial for the safety of ship structures. To make the local characteristics of trimaran load fluctuation easier to be matched by the LSTM neural network, the signal decomposition methods are adopted and selected in the research. The initial monitoring signal is decomposed by EMD, EEMD, CEEMDAN, and VMD, respectively. The sub-signal sequences of IMFs and residue at bow are shown in Fig. 12. In the EMD, the number of signal decomposition layer is 9. There are both 13 sub-signal sequences of IMFs obtained by using the EEMD and CEEMDAN decomposition. For the VMD, seven sub-signal sequences are also calculated for the load prediction of trimarans. The same data decomposition is also applied to the midship and stern signals.

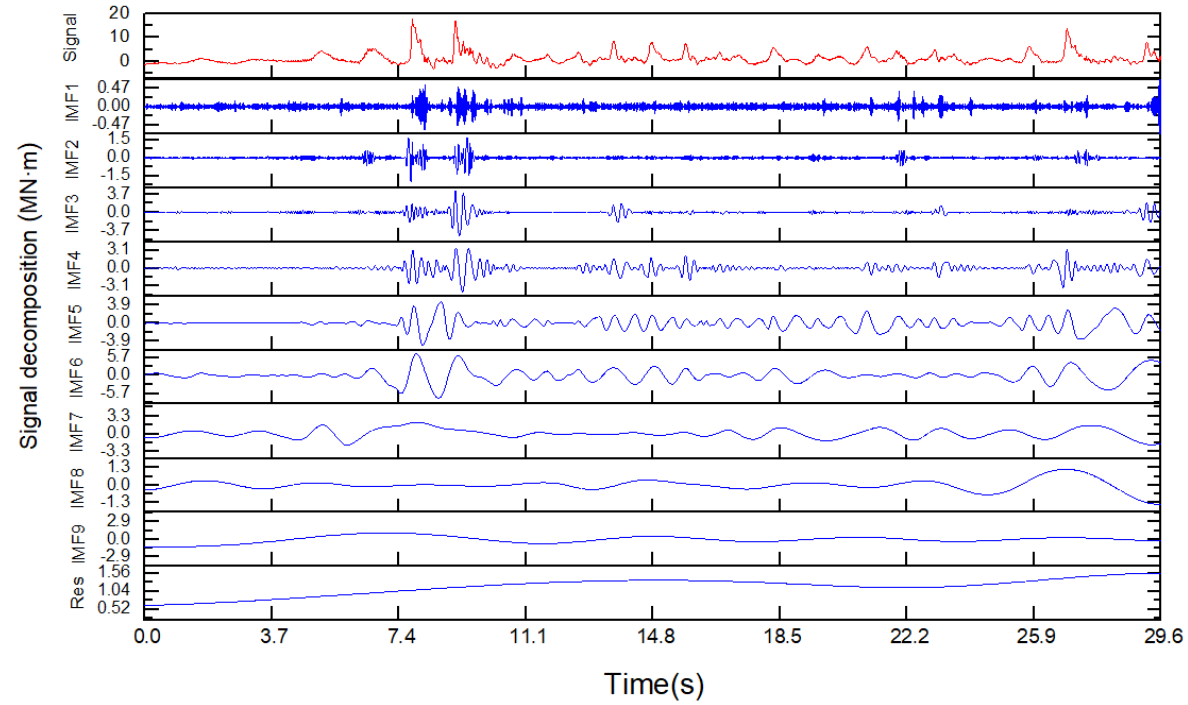

(a) Signal Decomposed results of EMD

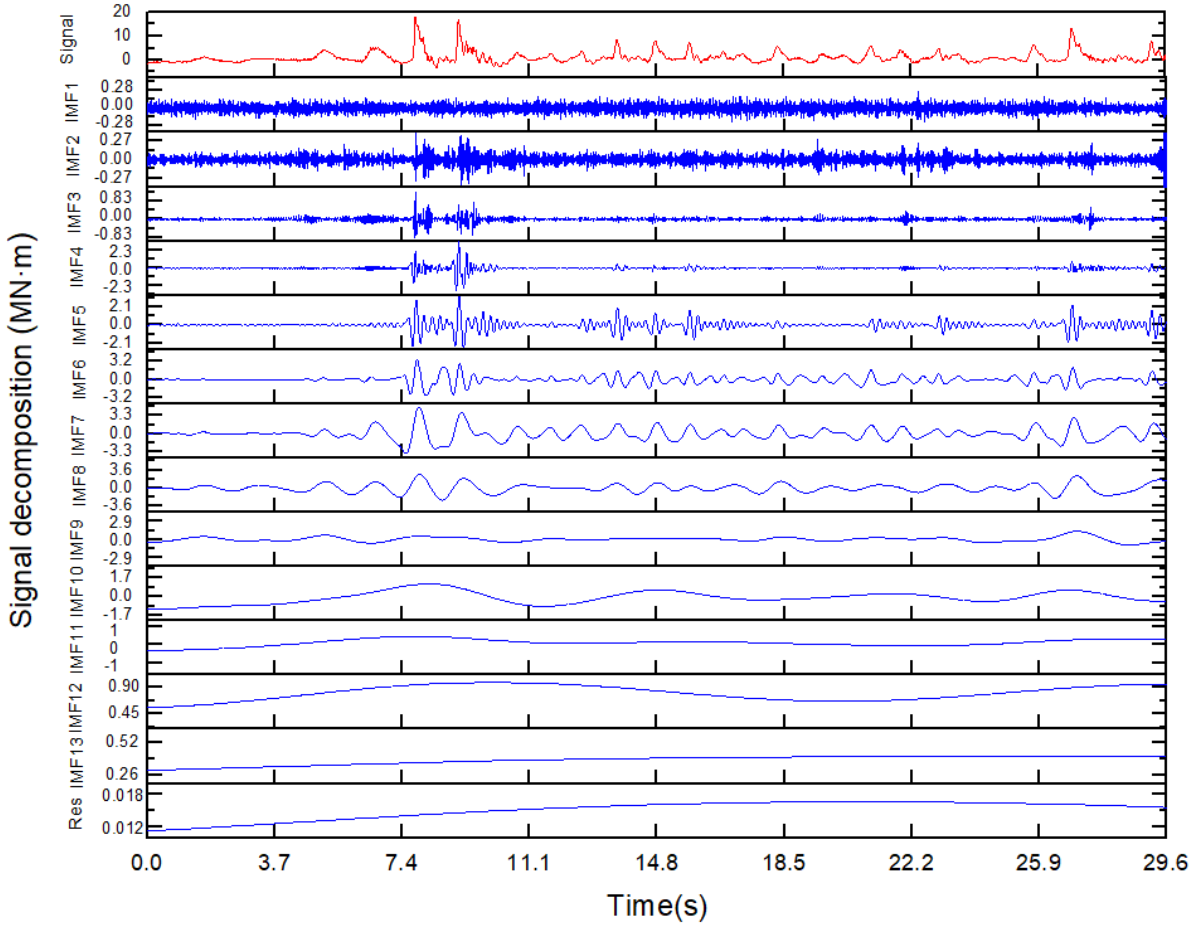

(b) Signal Decomposed results of EEMD

Fig. 12 Bow signal results with different signal decomposed methods

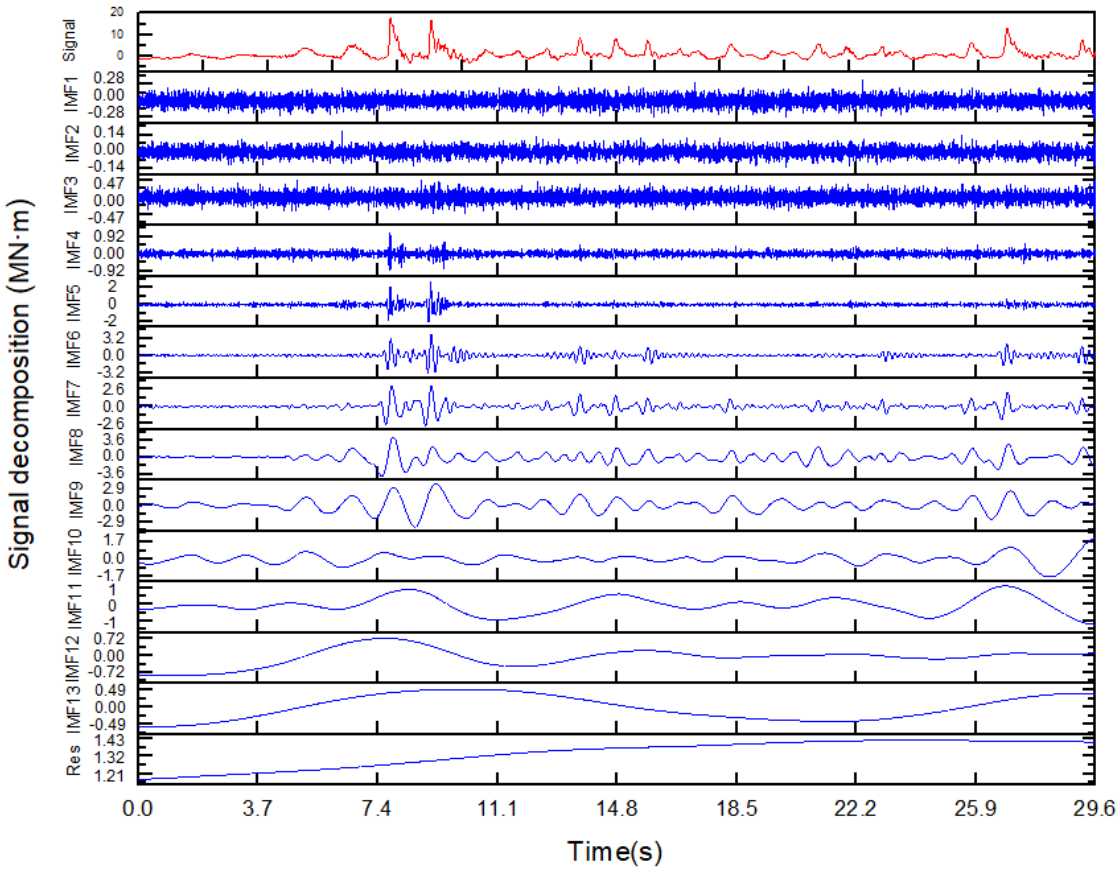

(c) Signal Decomposed results of CEEMDAN

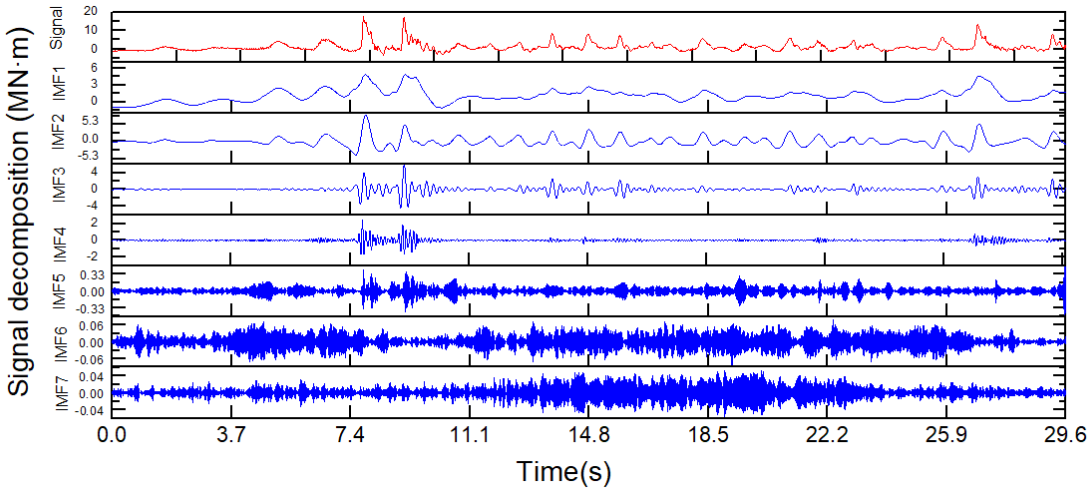

(d) Signal Decomposed results of VMD

Fig. 12 Bow signal results with different signal decomposed methods (continued)

In the signal decomposition, the high-frequency signal fluctuations are extracted by different IMFs from the monitoring signals. Then, these sub-signal sequences are multidimensional inputs of the LSTM neural network for training. Fig. 13 shows the trimaran load prediction fluctuations based on the LSTM neural network with different signal decomposition algorithms. The combined data-driven prediction models of EMD-LSTM, EEMD-LSTM, CEEMDAN-LSTM, and VMD-LSTM, both can achieve the goal of trimaran load forecasting. In the comparison with the original LSTM prediction, the load prediction based on these combined LSTM models reduce the phase deviation between the expectation and prediction. The prediction of load peak moment is more accurate in CEEMDAN-LSTM and VMD-LSTM models. In addition, the prediction in the local high-frequency signal fluctuations has been also improved, to some extent.

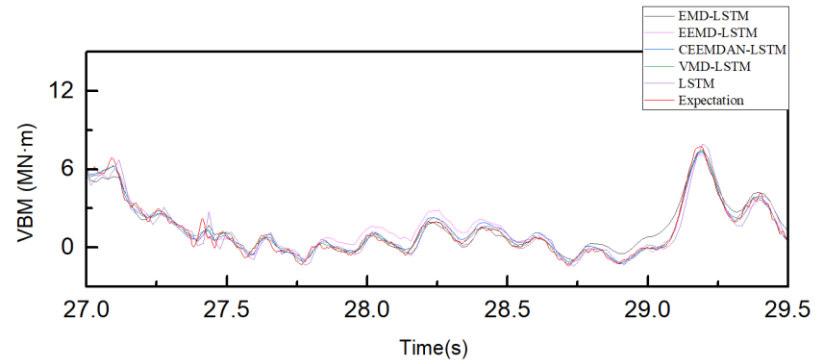

(a) Bow load prediction results with different combined prediction models

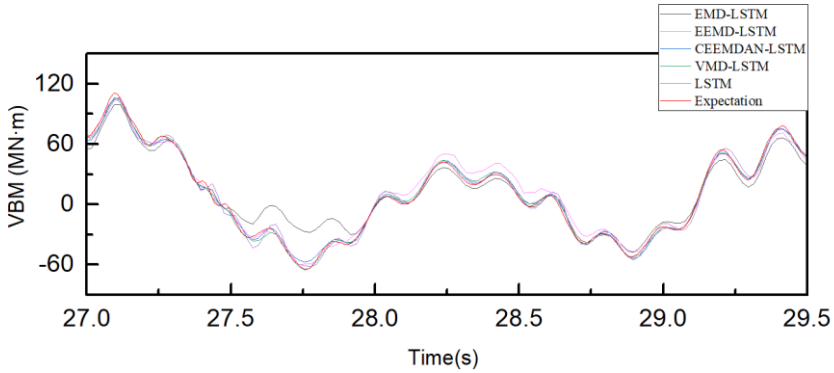

(b) Midship load prediction results with different combined prediction models

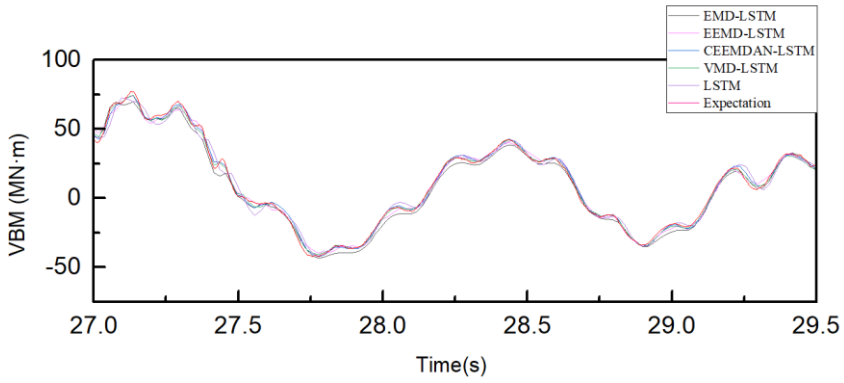

(c) Stern load prediction with different combined prediction models

Fig. 13 Trimaran load prediction results with different combined prediction models.

Fig. 14 summarizes the statistical results of the trimaran load prediction with different combined data-driven models. Although the R-squared correlation coefficients based on EMD-LSTM model are still higher than 0.9 at these three monitoring locations, the EMD algorithm cannot improve the trimaran load prediction. It is found the RRMSE of EMD-LSTM model is higher than that of the original LSTM model, especially at the trimaran midship where the significant fluctuation in amplitude often appears. For the EEMD-LSTM and CEEMDAN-LSTM models, their prediction accuracies both increase at bow and stern in comparison with the accuracy of the original LSTM model. The RRMSE of CEEMDAN-LSTM and EEMD-LSTM models decease by 47.47% and 25.28% at bow. The stern RRMSE of CEEMDAN-LSTM and EEMD-LSTM models also decease by 38.76% and 30.91%, respectively. At midship, the RRMSE of CEEMDAN-LSTM model only decease by 3.87%, while the RRMSE of EEMD-LSTM model grows by 19.55%. Due to the excessive emphasis on the high-frequency load fluctuation, the prediction ability of the EEMD-LSTM model weakens at midship, where there is a large proportion of low-frequency loads. The VMD-LSTM model shows a better predictive ability along the trimaran length. The deviation decline phenomenon is also found by the application

of VMD-LSTM model at three monitoring locations, and its decreasing proportions of RRMSE along ship length are 53.63%, 39.71%, and 47.18%. The R-squared correlation coefficient of VMD-LSTM model is also the highest among these combined load perdition models. Therefore, the VMD-LSTM model has advantages in the trimaran load perdition.

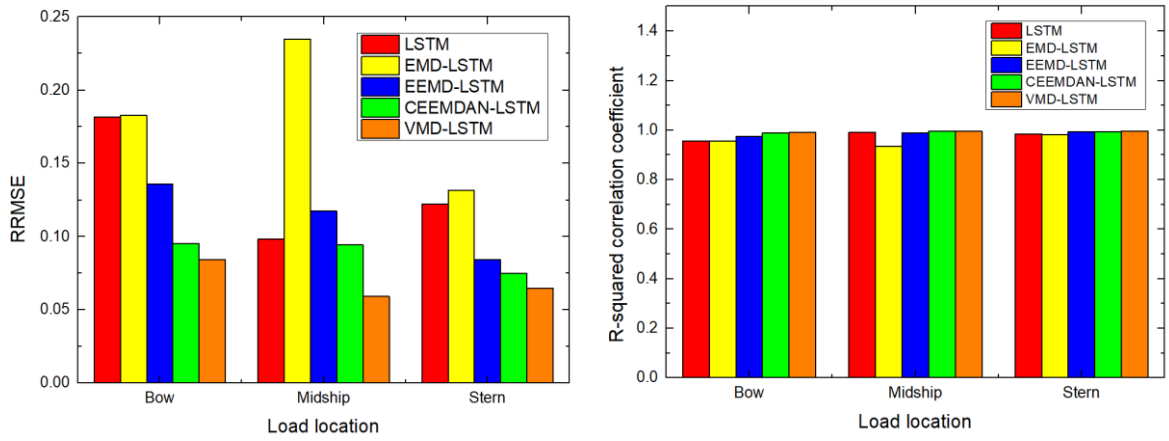

(a) Results of RMSE (b) Results of R-squared correlation coefficient

Fig. 14 Statistical indicators with different combined prediction models

To further investigate the details of the improvement in the load perdition accuracy by the VMD-LSTM model, Fig. 15 shows the deviation comparison between the original LSTM model and the VMD-LSTM model in trimaran load perdition. After the VMD application, the deviation between theoretical prediction and expectation has been wholly reduced. The load prediction of the VMD-LSTM model in both peaks and troughs is closer to the expectation in comparison with the prediction of the original LSTM model. For load peaks, the predicted value of the VMD-LSTM model is lower than the expectation, and the location of the max prediction deviation is bow. The trough prediction of the VMD-LSTM model is relatively more accurate at midship and stern. The maximum deviation ratio of the VMD-LSTM model is less than 9%. Obviously, the VMD-LSTM model can effectively predict the trimaran load fluctuations in short term.

To observe the load predictive performance of the VMD-LSTM model, its prediction scope is also studied. The number of output steps for VMD-LSTM changes, the theoretical predictions for 5-step ahead, 10-step ahead, 15-step ahead, and 20-step ahead, are taken respectively. Fig. 16 shows the VMD-LSTM prediction results with different output scopes.

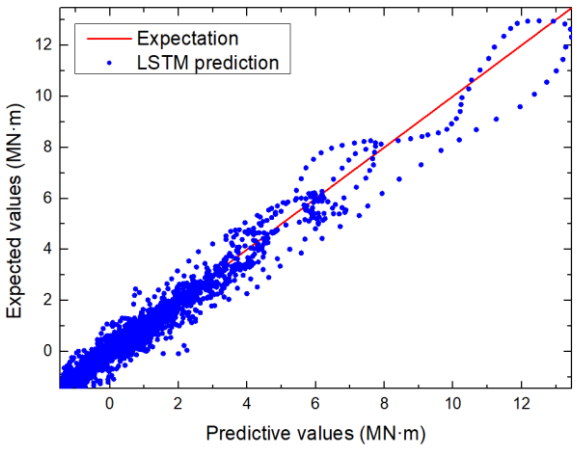

(a) Bow deviation in the LSTM prediction

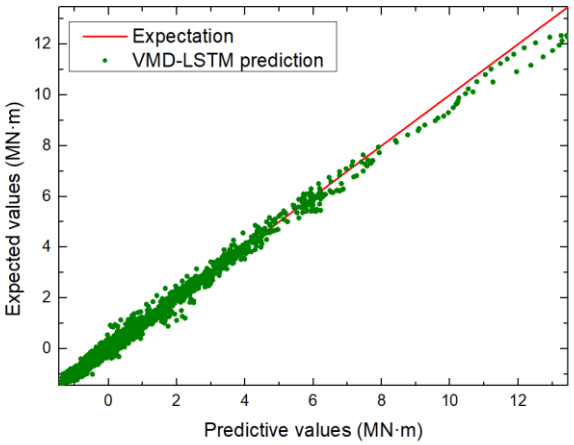

(b) Bow deviation in the VMD-LSTM prediction

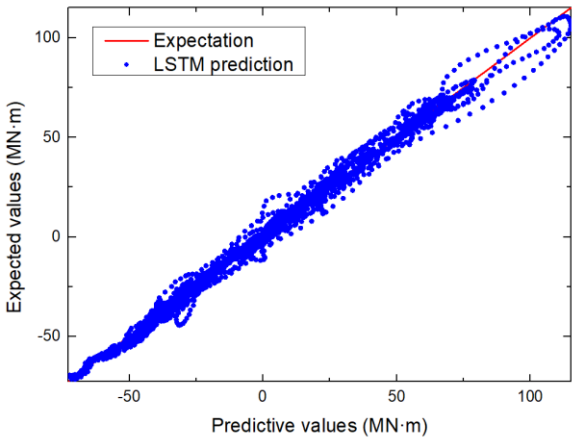

(c) Midship deviation in the LSTM prediction

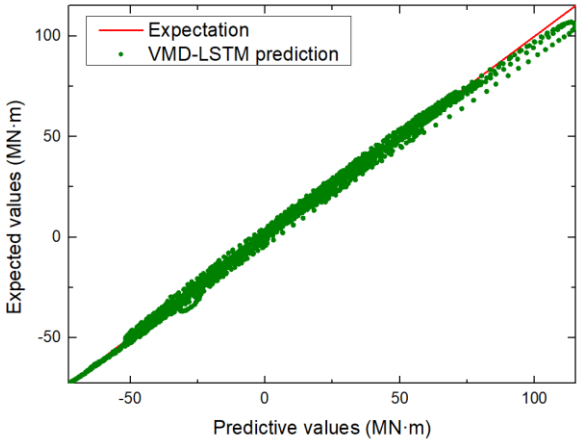

(d) Midship deviation in the VMD-LSTM prediction

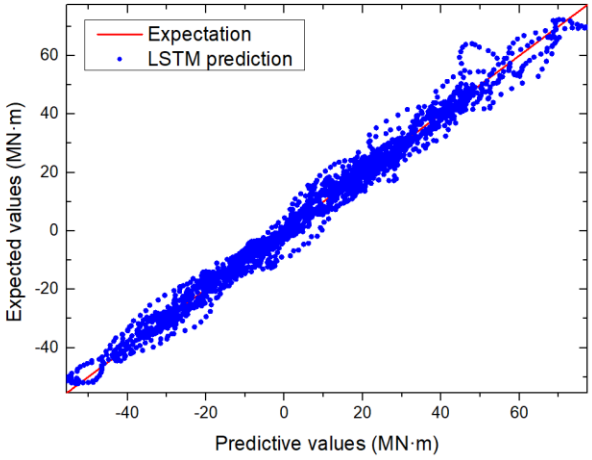

(e) Stern deviation in the LSTM prediction

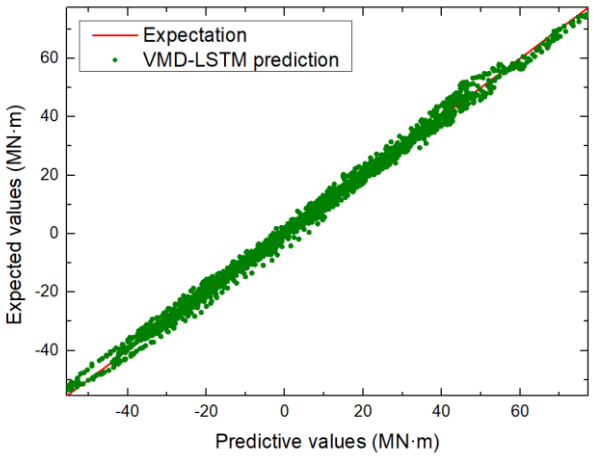

(f) Stern deviation in the VMD-LSTM prediction

Fig. 15 Load deviation comparison between the original LSTM model and the VMD-LSTM model

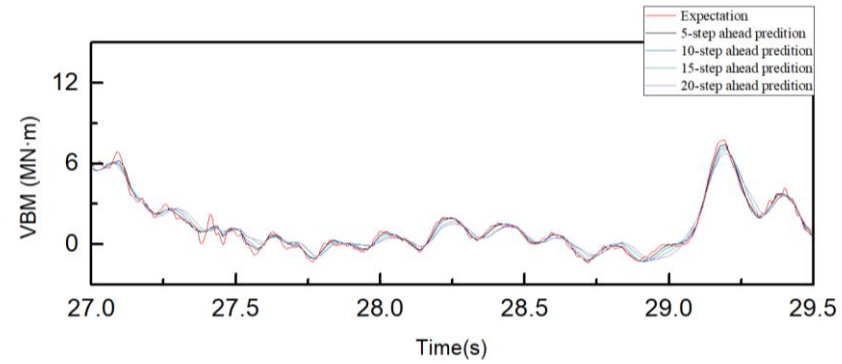

(a) Bow load prediction results with different output scopes

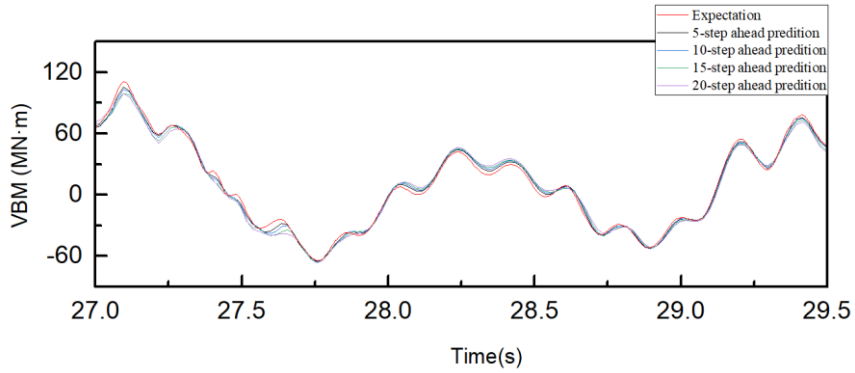

(b) Midship load prediction results with different output scopes

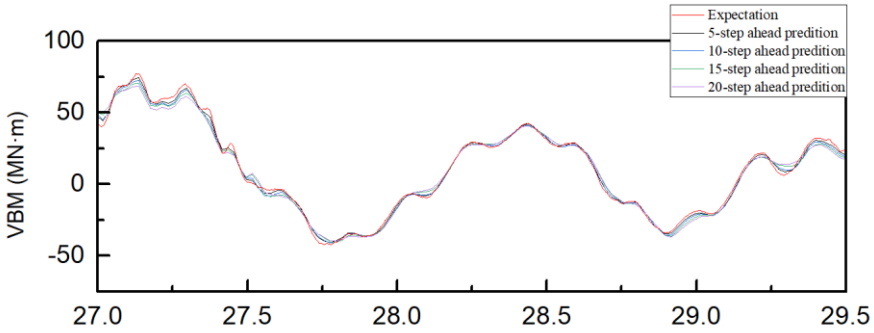

(c) Stern load prediction results with different output scopes

Fig. 16 VMD-LSTM prediction results with different output scopes.

Obviously, with the prediction scope of trimaran load growth, the predictive ability of the VMD-LSTM model gradually weakens. The deviation between the expectation and the prediction is wider in both amplitude and phase. The predicted peaks in the VMD-LSTM decreases at the longer output scopes, and the moment of predicted load fluctuations gradually delays from the 5-step ahead prediction to the 20-step ahead prediction.

Fig. 17 summarizes the statistical results of VMD-LSTM model with different prediction scopes. It is found that the RRMSE of the VMD-LSTM model at these monitoring positions both increases in the wider prediction scope. The increasing trend of the RRMSE at the trimaran midship shows a rough linear relationship, while the RRMSE growth of the trimaran bow and stern appear some different nonlinear characteristics. Through the comparative analysis on the R-squared correlation coefficients, it is found that the R-squared correlation coefficients of bow load are always lowest under the different output scopes. The nonlinear descent phenomenon of R-squared correlation coefficients is more pronounced at bow and stern. This phenomenon, which the accuracy of load prediction decreases with the growth of the prediction scope, has also been found in other load prediction models, as shown in Fig. 18. In the 20 step-ahead prediction, the R-squared correlation coefficients of the LSTM model along the trimaran length cannot reach 0.90, while the R-squared correlation coefficients of VMD-LSTM and CEEMDAN-LSTM models are both higher than 0.95. Obviously, the signal decomposition of VMD and CEEMDAN have a mitigating effect on the accuracy decreasing caused by the expansion of the step-ahead prediction range. It is also indicated that the RRMSE of

the VMD-LSTM model is still the smallest among these load prediction models, regardless of the prediction scopes.

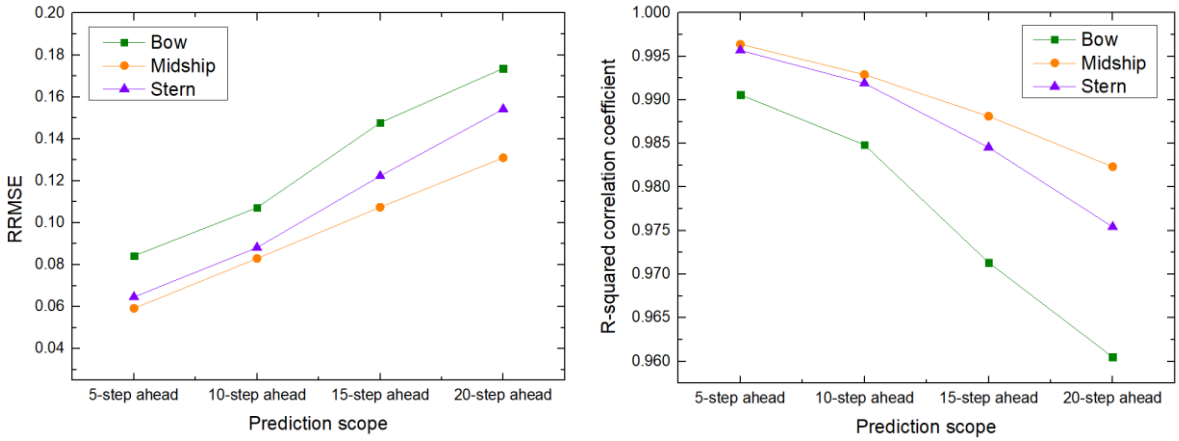

(a) Results of RRMSE (b) Results of R-squared correlation coefficient

Fig. 17 Statistical indicators of VMD-LSTM model at different prediction scopes.

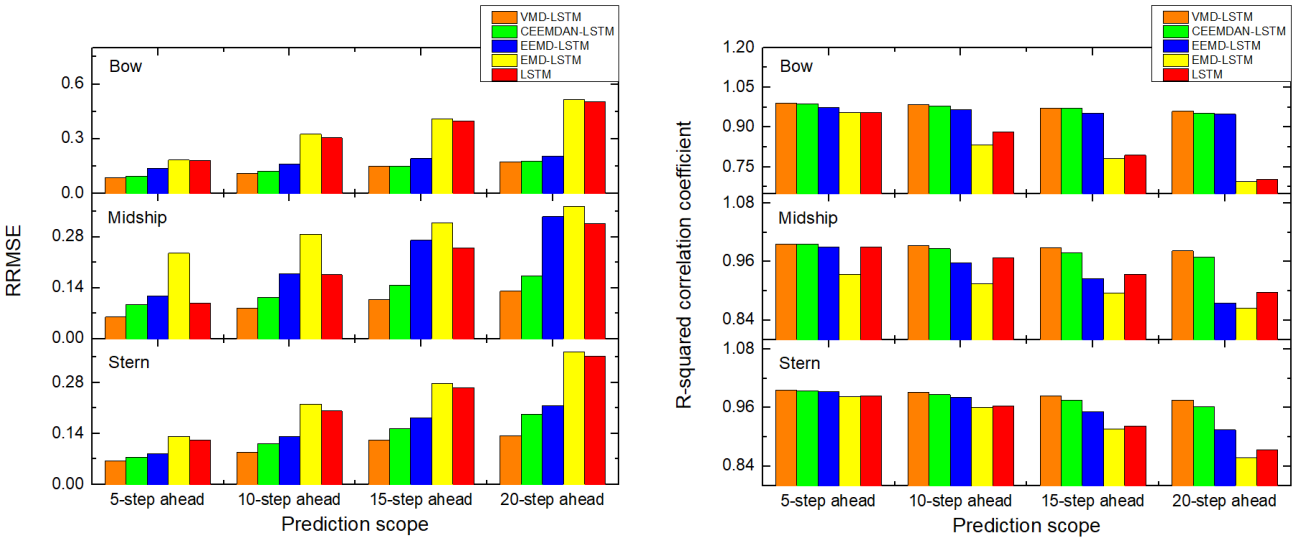

(a) Results of RRMSE (b) Results of R-squared correlation coefficient

Fig. 18 Statistical indicators of load prediction models at different prediction scopes.

4.5 Sensitivity analysis on load prediction model

To verify the reliability of VMD- LSTM model, the sensitivity analysis towards this data driven model is taken. The update strategy of LSTM neural network is adjusted to observe the changes in the load prediction accuracy. The VMD-LSTM model is only trained in the first sub-cases and not updated in subsequent sub-cases to further evaluate the forecasting capability for the load fluctuations at different time periods of the same wave conditions.

Fig. 19 shows the comparison of prediction accuracies under different strategies. Obviously, when the invariant strategy is adopted in the 5 step-ahead load prediction, the prediction accuracies at all monitoring locations decrease slightly, although their accuracies are higher than 0.97. The prediction accuracy has decreased by 1.37% at midship, and the relative decreasing magnitudes of prediction accuracies at bow and stern are 2.07% and 1.66%, respectively. The adjustment of update strategies is more sensitive to the bow and stern. When the prediction scope of trimaran load widens, the prediction accuracy under the invariant strategy also appears nonlinear downward trend. Although the accuracy deviation in these two strategies is wider with the prediction scope growth, the prediction accuracy of the invariant VMD-LSTM model for 20 step-ahead is

always higher than 0.93. Without the regular updates, this prediction model can still maintain relatively high forecasting accuracy to detect the trimaran load fluctuation in different time periods.

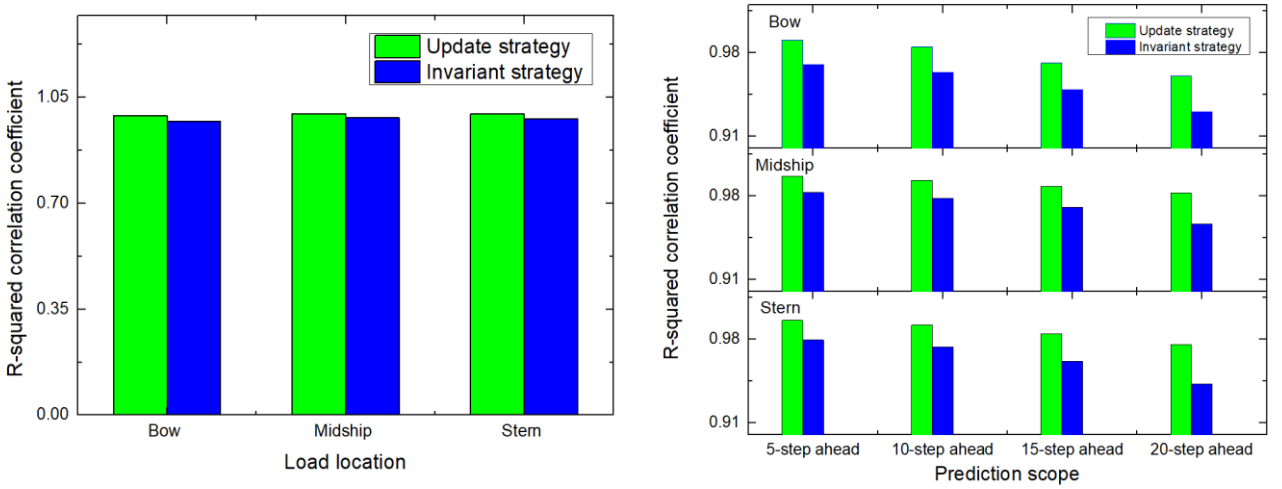

(a) Prediction accuracies in varied load locations (b) Prediction accuracies in varied prediction scopes

Fig. 19 Comparison of prediction accuracies under different strategies (case WI).

Then, the robustness of the VMD-LSTM prediction model on the varied irregular wave environment is investigated. Fig. 20 shows the statistical indicators of the load prediction model in different wave heights. It is found that the RRMSE and the R-squared correlation coefficients both appear fluctuation with small range under the varied wave heights. Because the load fluctuation at midship is most significant among these monitoring positions, the min RRMSE and the max R-squared correlation coefficient are found at midship. Therefore, the trimaran load prediction based on the VMD-LSTM model has higher accuracy at midship. In the case WII, it is indicated that the R-squared correlation coefficients at different wave heights are always higher than 0.98 under the 5-step ahead prediction. It is concluded that the VMD-LSTM model can effectively predict the short-term fluctuations in the varied wave heights.

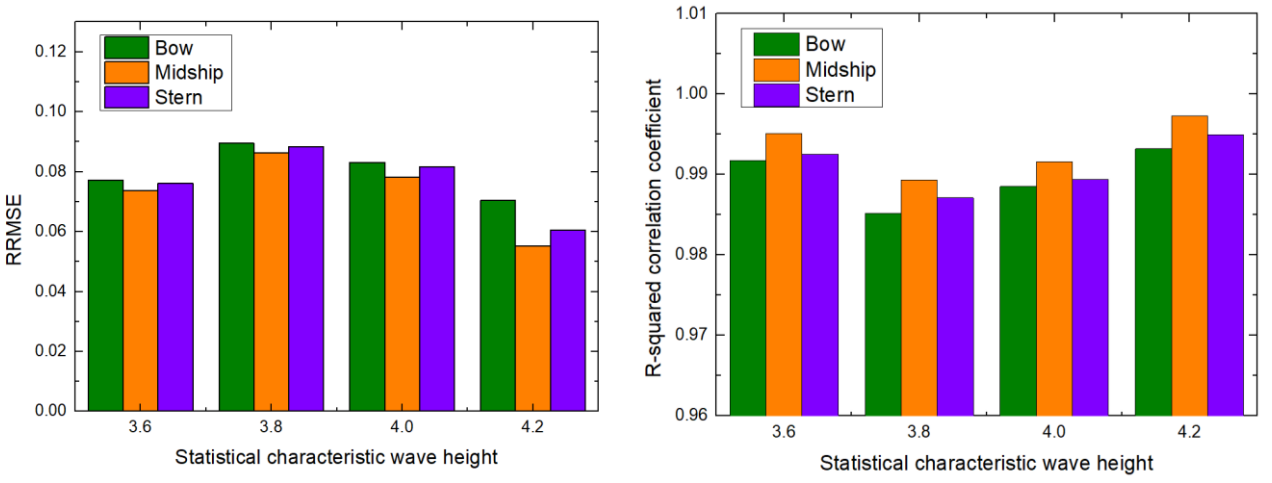

(a) Results of RRMSE (b) Results of R-squared correlation coefficient

Fig. 20 Statistical indicators of VMD-LSTM prediction model under varied wave heights (case WII).

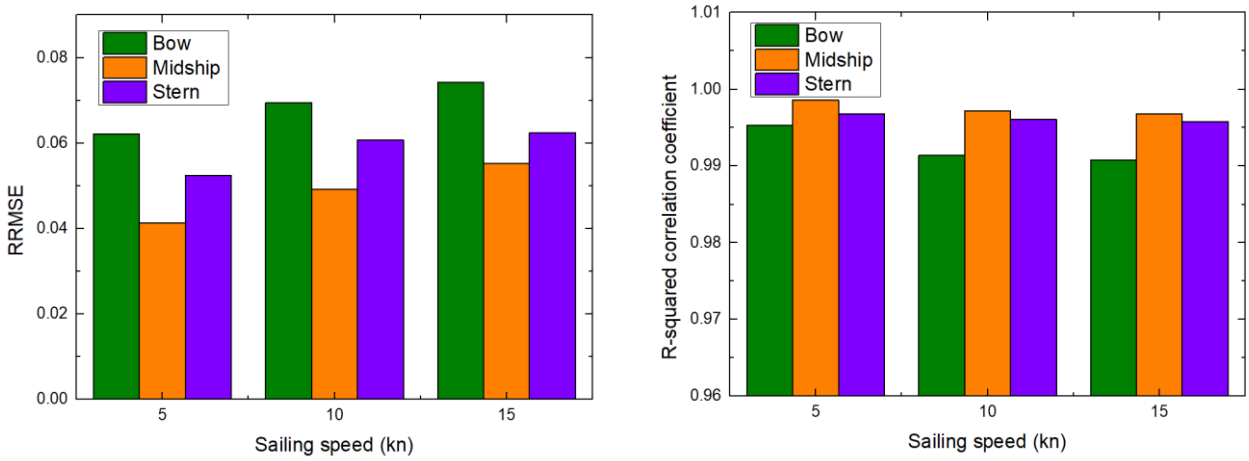

(a) Results of RRMSE (b) Results of R-squared correlation coefficient

Fig. 21 Statistical indicators of VMD-LSTM prediction model under varied sailing speeds (case WIII).

Due to the limitations of experimental equipment performance, the model tests with different sailing speeds are taken to extract the trimaran load characteristics at different encounter frequencies. Fig. 21 shows the statistical indicators of the load prediction model in varied sailing speeds. With the sailing speed increasing, the RRMSE and the R-squared correlation coefficients both grow with small range. The bow deviation of the load perdition is highest among these monitoring locations. In the case WIII, it is indicated that the R-squared correlation coefficients still maintain a high level at different speeds. Obviously, the VMD-LSTM prediction model has high stability when ship is suffering the wave impact with different encounter frequencies. Finally, it is concluded that the VMD-LSTM model can effectively predict the short-term fluctuations in the trimaran high-frequency loads with the varied marine environment. The application of the VMD-LSTM data-driven model will provide the reliable data support for structural health monitoring and damage detection of intelligent trimarans.

5. Conclusion

In the research, a method of trimaran load prediction in short-term is developed by using the data driven technology. According to the monitoring load data from a trimaran model test, the relevant parameters of the LSTM neural network are optimized, and the combined data-driven model is further established by combing the LSTM neural network with different signal decomposition algorithms. Finally, the following conclusions are drawn:

(1) In the data-driven model based on LSTM neural network, the influence of input length, neuron number, ANN optimizer, and output scope, cannot be ignored. The influence of input length on trimaran load prediction is varied with different monitoring positions, and the bow signals often require more input data to improve the prediction accuracy. The different neuron numbers also affect the prediction of high-frequency load peaks at bow, and its influence is relatively weaker than the influence of input length. The selection of ANN optimizer in the LSTM neural network should be taken more attention, and the Adam optimization algorithm has advantages in the trimaran load prediction. The output scope of the data-driven model is also related to the accuracy of trimaran load prediction. As the theoretical prediction range expands, the accuracy of the data-driven models in the trimaran load prediction will decrease.

(2) The signal decomposition algorithms are useful to establish the combined data-driven models for further improving the accuracy of trimaran load. In the comparison with the original LSTM model, the combined LSTM models can reduce the phase deviation between the expectation and prediction. The load predictions based on the VMD-LSTM model and the CEEMDAN-LSTM model are closer to the values of model test at different monitoring positions. It is also found that the data-driven VMD-LSTM model always has the highest prediction accuracy among these combined models, and its load prediction is most reliable at midship.

(3) The high stability of the trimaran load prediction is found in the VMD-LSTM model. With different model update strategies, wave heights, and sailing speeds, its R-squared correlation coefficients at different monitoring positions still maintain a high level and meet the general engineering requirement. Therefore, the short-term prediction based on the VMD-LSTM data-driven model is recommended in trimaran monitoring systems.

The current research is mainly based on the scaled model test, while some actual ship factors such as wind, crew activity and three-dimensional waves, are still ignored. In the future research, the monitoring data of actual ship will be collected and investigated. The optimized data-driven model will be further combined with the hull structural reliability theory to predict and evaluate the trimaran load and structural strength.

ACKNOWLEDGMENTS

This research is supported by the National Natural Science Foundation of China (No.52201353) and the Fundamental Research Funds for the Central Universities (No.3132024138). All authors express their gratitude to these foundations.

REFERENCES

[1] Jiang, Y., Sun, H., Zou, J., Hu, A., Yang, J., 2017. Experimental and numerical investigations on hydrodynamic and aerodynamic characteristics of the tunnel of planing trimaran. *Applied Ocean Research*, 63, 1-10. https://doi.org/10.1016/j.apor.2016.12.009

[2] Jiang, Z., Gao, Y., Liu, J., 2019. A lid approach for predicting wave induced motions of trimaran in regular waves. *Brodogradnja*, 70(2), 171-185. https://doi.org/10.21278/brod70209

[3] Khoob, A. A., Ketabdari, M. J., 2020. Short-term prediction and analysis of wave-induced motion and load responses of a wave-piercing trimaran. *Brodogradnja*, 71(2), 123-142. https://doi.org/10.21278/brod71208

[4] Tang, H., Wan, Q., Ren, H., 2023. Numerical study of trimaran wave load based on time-domain Rankine method. *Brodogradnja*, 74(3), 107-129. https://doi.org/10.21278/brod74306

[5] Zhang, Y. H., Hu, J. F., Ma, S., Wang, P., 2023. Anti-rolling analysis and resistance optimization of a new anti-rolling hydrofoil for the trimaran vessel. *Ocean engineering*, 272, 113837. https://doi.org/10.1016/j.oceaneng.2023.113837

[6] Li, Y., Tang, Z., Gong, J., 2023. The effect of PID control scheme on the course-keeping of ship in oblique stern waves. *Brodogradnja*, 74(4), 155-178. https://doi.org/10.21278/brod74408

[7] Mentes, A., Yetkin, M., 2022. An application of soft computing techniques to predict dynamic behaviour of mooring systems, *Brodogradnja*, 73(2), 121-137. https://doi.org/10.21278/brod73207

[8] Yildiz, B., 2022. Prediction of residual resistance of a trimaran vessel by using an artificial neural network. *Brodogradnja*, 73(1), 127-140. https://doi.org/10.21278/brod73107

[9] Kaplan, P., 1969. A study of prediction techniques for aircraft carrier motions at sea. *Journal of Hydronautics*, 3(3), 121-131. https://doi.org/10.2514/3.48101

[10] Zeng, Q., 2008, Modelling and prediction of ship motion attitude based on the neural network. Master thesis, *Harbin Engineering University*, Harbin, China.

[11] Sun, Q., Tang, Z., Gao, J., Zhang, G., 2022. Short-term ship motion attitude prediction based on LSTM and GPR. *Applied Ocean Research*, 118, 102927. https://doi.org/10.1016/j.apor.2021.102927

[12] Presti, J.L., Magni, L., Toffanin, C., 2023. Ship manoeuvering modelling with a physics-oriented neural network-based approach. *IFAC-Papers on Line*, 56(02), 3471-3476. https://doi.org/10.1016/j.ifacol.2023.10.1500

[13] Jiang, Z., Ma, Y., Li, W., 2024. A data-driven method for ship motion forecast. *Journal of Marine Science and Engineering*. 12(2), 291. https://doi.org/10.3390/jmse12020291

[14] Gao, N., Chuang, Z., Hu, A., 2024. Real-time prediction of ship motion based on improved empirical mode composition and dynamic residual neural network. *Ocean Engineering*, 292, 116528. https://doi.org/10.1016/j.oceaneng.2023.116528

[15] Chojaczyk, A. A., Teixeira, A. P., Neves, L. C., Cardoso, J. B., Soares, C. G., 2014. Review and application of artificial neural networks models in reliability analysis of steel structures. *Structural Safety*. 52(03), 78-89. https://doi.org/10.1016/j.strusafe.2014.09.002

[16] Wu, S., Jiao, S., 2018. Prediction of stress pattern in the ship structure monitoring system. *Applied Science and Technology*, 45(6), 8-11.

[17] Chao, L., 2022. Research on ship wave load forecast method based on long short-term memory network algorithm. Master thesis, *Harbin Engineering University*, Harbin, China.

[18] Tang, H., Zhu, R., Wan, Q., Ren, D., Meng, J., 2023. Prediction of ship structure response signal based on Bo-LSTM neural network, 6th *IEEE International Conference on Unmanned Systems*, 13-15 October, 2023, Hefei, China. https://doi.org/10.1109/ICUS58632.2023.10318384

[19] Wang, Q., Yu, P., Lv, M., Wu, X., Li C., Chang, X., Wu, L., 2024. Real-time prediction of wave-induced hull girder loads for a large container ship based on the recurrent neural network model and error correction strategy, *International Journal of Naval Architecture and Ocean Engineering*, 16, 100587. https://doi.org/10.1016/j.ijnaoe.2024.100587

[20] Wang, Q., Wu, L., Li, C., Chang, X., Zhang, B., 2024. Research on a Real-Time Prediction Method of Hull Girder Loads Based on Different Recurrent Neural Network Models. *Journal of Marine Science and Engineering*, 12(5), 746. https://doi.org/10.3390/jmse12050746

[21] Tang, H., He, Z., Zhang, X., Wan, Q., 2023. Autonomous recognition of a ship structure characteristic signal based on machine learning. *International Journal of Offshore and Polar Engineering*. 33(2), 174–183. https://doi.org/10.17736/ijope.2023.mt34

[22] Fan, G., Yu, P., Wang, Q., Dong, Y., 2023. Short-term motion prediction of a semi-submersible by combining LSTM neural network and different signal decomposition methods. *Ocean engineering*, 267, 113266. https://doi.org/10.1016/j.oceaneng.2022.113266

[23] Huang, N. E., Shen, Z., Long, S. R., Wu, M. C., Shih, H. H., Zheng, Q., Yen N., Tung C., Liu H. H., 1998. The empirical mode decomposition and the Hilbert spectrum for nonlinear and non-stationary time series analysis. *Proceedings of the Royal Society of London Series A*, 454, 903-995. https://doi.org/10.1098/rspa.1998.0193

[24] Hu, A., Sun J., Xiang L., 2011. Mode mixing in empirical mode decomposition. *Journal of Vibration, Measurement & Diagnosis*, 31(4), 429-434.

[25] Dragomiretskiy, K., Zosso, D., 2014. Variational mode decomposition. *IEEE Transactions on Signal Processing*, 62(3), 531-544. https://doi.org/10.1109/TSP.2013.2288675

[26] Wang, Z., Qiao, D., Yan, J., Tang, G., Li, B., Ning, D., 2022. A new approach to predict dynamic mooring tension using LSTM neural network based on responses of floating structure. *Ocean engineering*, 249, 110905. https://doi.org/10.1016/j.oceaneng.2022.110905

[27] Hochreiter, S., Schmidhuber, J., 1997. Long short-term memory. *Neural Computation*, 9(8), 1735-1780. https://doi.org/10.1162/neco.1997.9.8.1735

[28] Bi C., Yuan X., 2021. Deep learning training via distributed approximate newton-type method based on Adam local optimization. *Computer Applications and Software*, 38(10), 278-283.

[29] Tang, H., Ren, H., Zhong, Q., 2019, Design and model test of structural monitoring and assessment system for trimaran. *Brodogradnja*, 70(2), 111-134. https://doi.org/10.21278/brod70206

[30] Tang, H., Ren, H., Li, H., 2016. Experimental investigation of wave-induced hydroelastic vibrations of trimaran in oblique irregular waves. *Shock and Vibration*, 2016, 1-17. https://doi.org/10.1155/2016/8794560

[31] Jiao, J., Sun, S., Ren, H., 2016. Predictions of wave induced ship motions and loads by large-scale model measurement at sea and numerical analysis. *Brodogradnja*, 67, 81-100. https://doi.org/10.21278/brod67206

[32] Martić, I., Degiuli, N., Grlj, C.G., 2023. Prediction of added resistance of container ships in regular head waves using an artificial neural network. *Journal of Marine Science and Engineering*. 11(7), 1293. https://doi.org/10.3390/jmse11071293

[33] He, G., Yao, C., Sun, X., Meng, F., 2024, Research on ship motion prediction method based on coupled feature LSTM. *Journal of Huazhong University of Science and Technology*, 52(4), 1-7.